NEOPLASIA
www.neoplasia.com

Volume 15 Number 4 April 2013 pp. 384–398 384

Deconstruction of Medulloblastoma Cellular Heterogeneity Reveals Differences between the Most Highly Invasive and Self-Renewing Phenotypes[1,2]

Ludivine Coudière Morrison*,[3], Robyn McClelland*,[3], Christopher Aiken*, Melissa Bridges*, Lisa Liang*, Xin Wang†, Domenico Di Curzio‡, Marc R. Del Bigio‡, Michael D. Taylor† and Tamra E. Werbowetski-Ogilvie*

*Regenerative Medicine Program, Department of Biochemistry and Medical Genetics, University of Manitoba, Winnipeg, Manitoba, Canada; †Arthur and Sonia Labatt Brain Tumour Research Centre and Program in Developmental and Stem Cell Biology, The Hospital for Sick Children, Toronto, Ontario, Canada; ‡Department of Pathology, University of Manitoba and Manitoba Institute of Child Health, Winnipeg, Manitoba, Canada

Abstract

Medulloblastoma (MB) is the most common malignant primary pediatric brain tumor. Major research efforts have focused on characterizing and targeting putative brain tumor stem or propagating cell populations from the tumor mass. However, less is known about the relationship between these cells and highly invasive MB cells that evade current therapies. Here, we dissected MB cellular heterogeneity and directly compared invasion and self-renewal. Analysis of higher *versus* lower self-renewing tumor spheres and stationary *versus* migrating adherent MB cells revealed differential expression of the cell surface markers CD271 [p75 neurotrophin receptor (p75NTR)] and CD133. Cell sorting demonstrated that CD271 selects for subpopulations with a higher capacity for self-renewal, whereas CD133 selects for cells exhibiting increased invasion *in vitro*. CD271 expression is higher in human fetal cerebellum and primary samples of the Shh MB molecular variant and lower in the more aggressive, invasive group 3 and 4 subgroups. Global gene expression analysis of higher *versus* lower self-renewing MB tumor spheres revealed down-regulation of a cell movement transcription program in the higher self-renewing state and a novel potential role for axon guidance signaling in MB-propagating cells. We have identified a cell surface signature based on CD133/CD271 expression that selects for MB cells with a higher self-renewal potential or invasive capacity *in vitro*. Our study underscores a previously unappreciated role for CD271 in selecting for MB cell phenotypes and suggests that successful treatment of pediatric brain tumors requires concomitant targeting of a spectrum of transitioning self-renewing and highly infiltrative cell subpopulations.

Neoplasia (2013) 15, 384–398

Abbreviations: MB, medulloblastoma; TPC, tumor-propagating cell; BTPC, brain tumor–propagating cell; GBM, glioblastoma multiforme

Address all correspondence to: Dr Tamra E. Werbowetski-Ogilvie, Regenerative Medicine Program, Department of Biochemistry and Medical Genetics, University of Manitoba, 611-745 Bannatyne Avenue, Winnipeg, Manitoba, Canada, R3E 0J9. E-mail: ogilviet@cc.umanitoba.ca

[1]This work was funded by the Brain Tumour Foundation of Canada, the Health Sciences Centre Foundation, and the Manitoba Health Research Council. T.E.W.-O. holds a Canada Research Chair in Human Stem Cells and Neuro-oncology. M.R.D.B. holds a Canada Research Chair in Developmental Neuropathology. The authors declare no conflict of interest.

[2]This article refers to supplementary materials, which are designated by Tables W1 to W4 and Figures W1 to W3 and are available online at www.neoplasia.com.

[3]These authors contributed equally to this work.

Received 8 January 2013; Revised 5 February 2013; Accepted 6 February 2013

DOI 10.1593/neo.13148

Introduction

Medulloblastoma (MB) is the most common malignant primary pediatric brain tumor [1,2]. Classified as grade IV embryonal tumors of the central nervous system by the World Health Organization, MBs are derived from the neuronal lineage and exhibit dysregulation of several pathways associated with primitive neuroectoderm development including Wnt, Hedgehog, and Notch signaling [1,2]. Following surgery and treatment with chemotherapy and radiation, MBs often recur as a consequence of tumor cell infiltration into normal tissue and frequent metastasis through the cerebral spinal fluid [1–3]. Despite numerous advances in understanding the molecular basis for the malignant state and a 5-year survival rate of 60% to 70% [1], children with MB suffer from permanent cognitive and physical dysfunction attributed to the impact of toxic therapies on their developing nervous system [1].

Cancer stem cell theory suggests that a rare subpopulation of cells exhibit stem cell properties such as self-renewal capacity and multilineage differentiation [4,5]. These cancer stem cells or tumor-propagating cells (TPCs) would ultimately drive tumorigenesis and must be specifically targeted to abrogate malignant progression. Singh et al. demonstrated that a small subpopulation of brain tumor cells that express CD133 cell surface marker exhibit enhanced self-renewal capacity [6,7]. This work firmly established the existence of a "stem cell–like" phenotype within malignant brain tumors. However, more recent studies have shown that CD133– and CD133+ cells exhibit self-renewal capacity, while CD133– cells can generate more aggressive tumors *in vivo* [8–12]. Other studies have demonstrated that the cell surface marker CD15/SSEA1 selects for MB TPC populations in murine models [13,14]. Given the wide expression of CD133 in many tissues, it will be necessary to break down the heterogeneity within CD133+/– populations to identify other markers that also select for aggressive phenotypes. This is further complicated by recent demonstrations that interconversion of cancer cells between various differentiation states enables reestablishment of cellular equilibrium irrespective of the cell surface markers used to sort subpopulations [15]. Indeed, sorted cell fractions are not static and will inevitably give rise to other phenotypes in response to appropriate microenvironmental cues.

Most work on malignant brain tumor cell invasion and TPCs has been mutually exclusive despite the fact that TPCs and invasive cells share many cellular and molecular features including resistance to radiation and chemotherapy [16–22]. While some recent studies have directly addressed the relationship between invasive carcinoma cells and TPC populations [23,24], the specific relationship between TPCs and invasion in brain tumors is less concrete. CD133 has typically been used as a putative brain tumor–propagating cell (BTPC) marker [7]; however, recent work has shown that CD133– cells display more aggressive behavior than the CD133+ cells associated with "stem cell" function [9,12]. Chen et al. demonstrated that a more primitive CD133– subpopulation of glioblastoma multiforme (GBM) cells gives rise to both CD133– and CD133+ subsets. Further validating this work is the finding that GBM stem cell populations selected on the basis of "side population" or Hoechst 33342 dye exclusion actually exhibit decreased migration [25]. In contrast, other reports have shown that invasive and tumor mass or "core" GBM cells exhibit self-renewal capacity and stem cell marker expression; however, the stem cell features are more pronounced in the invasive population [26].

To date, there are no studies directly examining the specific relationship between BTPCs and the highly invasive subpopulation in pediatric brain tumor cells. Here, we tested the hypothesis that dissection of MB cellular heterogeneity would reveal phenotypic differences between the highly self-renewing and invasive phenotypes. To this end, we deconstructed heterogeneous MB cultures and identified novel functional relationships among cells expressing CD133 and CD271 using an *in vitro* model system. Higher self-renewing cells exhibit a CD271↑, CD133↓ cell surface signature, whereas a highly motile cell displays CD271↓, CD133↑ phenotype. This was supported by down-regulation of the cell motility transcription program in our highly self-renewing tumor spheres in stem cell conditions. Our study has identified a previously unappreciated role for CD271 in selecting for MB cell types and suggests that successful treatment of MB will require targeting of transitioning self-renewing and highly infiltrative MB subpopulations expressing several phenotypic markers.

Materials and Methods

Cell Culture and Maintenance

Daoy human MB cells (originally derived from a desmoplastic cerebellar MB) and D283 cells were purchased from the American Type Culture Collection (ATCC, Rockville, MD). Cells were cultured in Eagle's minimum essential media (EMEM) (ATCC) containing 10% FBS (Fisher Scientific, Ottawa, Ontario). Upon reaching confluency, cells were dissociated in Accutase (Invitrogen, Burlington, Ontario) and passed 1:15. Neural precursors from normal human embryonic stem cells called hENs and their transformed MB-like derivatives (t-hENs) were cultured as previously described [27]. Briefly, cells were dissociated for 5 minutes in Accutase and replated onto poly-L-lysine/laminin–coated plates (BD Biosciences, Mississauga, Ontario) in neural proliferation media [Dulbecco's modified Eagle's medium (DMEM)/F12 supplemented with 1% N2 (Gibco, Burlington, Ontario), 1% B27 (Gibco), 20 ng/ml epidermal growth factor (EGF; R&D Systems, Minneapolis, MN), and 20 ng/ml basic fibroblast growth factor (bFGF)]. Cells were passed every 5 days with media changes every 3 days.

For subclone expansion, Daoy MB cells were dissociated and resuspended in Dulbecco's phosphate-buffered saline (DPBS; Fisher Scientific) containing 0.5% FBS. A MoFlo XDP (Beckman Coulter, Inc, Mississauga, Ontario) cell sorter was used to deposit single Daoy cells into each well of a 96-well plate. These cells were subsequently cultured in EMEM with 10% FBS and expanded. Aliquots of 2.5×10^4 cells were prepared as hanging drops in 20 μl as previously described [28,29]. Hanging drops were incubated for 3 days to form spheroids and then transferred to collagen type I gels (VWR, Mississauga, Ontario) prepared as previously described [29]. Following collagen gelation at 37°C, embedded spheroids were then overlain with EMEM containing 10% FBS. Spheroid measurements were taken at day 0 and invasion was measured at 72 hours (day 3) using a Zeiss Primo Vert microscope with micrometer. Individual Daoy subclones were characterized on the basis of their invasive capacity.

Flow Cytometry Cell Surface Marker Screen

Daoy subclones were dissociated, washed with DPBS, and cultured as tumor spheres in ultralow attachment plates with DMEM/F12 containing 1% B27, 1% N2, 20 ng/ml EGF, and 20 ng/ml bFGF. On day 4, tumor spheres were fed by removal and replacement of 1 ml of media. On day 7, Daoy tumor spheres were dissociated, washed, and resuspended in DPBS containing 0.5% FBS. Cells were counted using an automated cell counter (Bio-Rad, Mississauga, Ontario) or hemocytometer. Cells were then stained with one of the

following antibodies: CD44-FITC, CD30-FITC, CD184-PE, CD26-FITC, CD271–Alexa Fluor 647, CD133-PE, CD15-APC, or CD24-PE. All antibodies were obtained from BD Biosciences, with the exception of CD133 (Miltenyi Biotec, Cambridge, MA). Flow cytometry was performed on the MoFlo XDP cell sorter and analyzed using FlowJo software (Tree Star Inc, Ashland, OR).

Daoy Core and Migrating Cell Dissections

Daoy MB cells were prepared as hanging drops as previously described [28,29]. After 3 days of incubation, resulting spheroids were transferred into a plate containing EMEM with 10% FBS. Spheroids were incubated for 2 days, at which time the "core" was mechanically dissected from the migrating cells. The dissected cores as well as the remaining migrating cells were dissociated separately, resuspended in DPBS with 0.5% FBS, and stained with antibodies for CD44, CD30, CD184, CD26, CD271, CD133, CD15, and CD24 for analysis by flow cytometry.

Fluorescence-activated Cell Sorting

Day 7 passage 2 Daoy tumor spheres were pooled, dissociated, and counted using an automatic cell counter and stained for CD133 and CD271. Sort samples were also stained with 7AAD viability dye (Beckman Coulter, Inc). Cells were sorted on the basis of CD133/CD271 using a MoFlo XDP cell sorter. Analysis of cell sorting was performed using FlowJo software. Collected cell fractions were centrifuged and counted for subsequent functional assays.

For tumor sphere assays, aliquots of 2500 cells from each subpopulation were plated in a 24-well low attachment plates in DMEM/F12 containing 1% B27, 1% N2, 20 ng/ml EGF, and 20 ng/ml bFGF. Cells were incubated for 5 days, after which tumor spheres were counted. Tumor spheres from each population were then counted and replated in aliquots of 2500 cells for secondary tumor sphere assays.

For cumulative cell counts, aliquots of 2500 cells from each subpopulation were plated in a 24-well tissue culture plate in EMEM containing 10% FBS. Cells were fed on day 3, and on day 4, they were dissociated and counted using a hemocytometer to obtain cumulative cell counts.

For invasion assays, aliquots of 1.5×10^4 to 2.5×10^4 of sorted cell fractions were prepared as hanging drops and embedded in a type I collagen matrix as described. Measurements were taken on day 0 and day 3. Images were taken using a Nikon Eclipse TS100 microscope and Nikon DS-Fi1 Digital Sight camera (Nikon, Mississauga, Ontario).

Intracerebral Transplantations and Histology

The University of Manitoba Animal Care Committee approved all procedures and protocols. CD271+/CD133–, CD271–/CD133–, and unsorted Daoy tumor spheres were intracerebrally injected into non-obese diabetic severe combined immunodeficient (NOD/SCID) mice as previously described [7,27]. Briefly, mice were anesthetized with isoflurane and injected in the right frontal lobe with biologic replicates consisting of 2×10^5 CD271+/CD133–, CD271–/CD133–, and unsorted Daoy tumor spheres. After 7.5 weeks, animals were perfused with formalin and the brains were extracted, placed in formalin for 2 to 7 days, embedded in paraffin, and then sectioned (5-μm thickness). Sections were dewaxed in xylene and rehydrated through a graded series of alcohol concentrations. Samples were stained with hematoxylin and eosin. Slides were mounted and imaged using an EVOS xl core microscope (AMG, Seattle, WA). Malignant cell growth was scored, from a scale of 0 to 3, where 0 = no malignant cells with certainty, 1 = indicates rare clusters of malignant cells confined to subarachnoid compartment, 2 = malignant cells in subarachnoid compartment and infiltrating perivascular spaces, and 3 = features in 2, in addition to tumor nodules growing in other areas of the brain or cerebellum. For each tumor sample, two slides containing six to seven brain sections were scored and averaged to obtain a grade. Slides were assessed by a neuropathologist who was blinded to cellular identity.

5-Fluorouracil Treatment

Daoy passage 1 tumor spheres were plated in six-well low attachment plates at a cell density of 1×10^5 cells per well, in duplicate. Concentrations of 0.5, 1.0, and 2.5 μg/ml 5-fluorouracil (5-FU; Sigma, Oakville, Ontario) as well as a DMSO control were used. Cells were plated on day 0, and then after 7 days, samples were dissociated and half were collected for flow cytometry analysis of CD133/CD271 or viability using the Annexin V Apoptosis Kit (BD Biosciences). The remaining samples were replated in fresh neural precursor media or fresh neural precursor media with various concentrations of 5-FU. Samples were then collected and analyzed again at day 14.

Quantitative Reverse Transcription–Polymerase Chain Reaction

Core and migrating cell populations were subjected to quantitative polymerase chain reaction (qPCR) analysis of Otx2, Sox1, βIII tubulin, EPHB1, EPHB2, EPHB3, EPHB4, EPHB6, and ephrin B2 transcript levels. Total RNA was extracted using the AllPrep DNA/RNA Mini Kit (Qiagen, Mississauga, Ontario) according to the manufacturer's guidelines. First-strand cDNA was synthesized using the Superscript III First Strand Synthesis System (Invitrogen). The following PCR conditions were used: 50°C for 2 minutes, 95°C for 2 minutes, and 40 cycles of 95°C for 15 seconds and 60°C for 30 seconds. qPCR was conducted using Platinum SYBR Green qPCR SuperMix-UDG (Invitrogen) or GoTaq qPCR Master Mix (Fisher Scientific) and performed on an Mx3000P (Stratagene, Santa Clara, CA) qPCR system. All values were normalized to glyceraldehyde 3-phosphate dehydrogenase (GAPDH). Specific primer sequences for each gene are listed in Table W4.

Global Gene Expression Profiling

Total RNA was isolated from higher *versus* lower self-renewing Daoy MB tumor spheres, using the All-in-One Purification Kit (Norgen Biotek, Thorold, Ontario) according to the manufacturer's instructions. RNA amplification and GeneChip 3′ oligonucleotide microarray hybridization and processing were performed by the London Regional Genomics Centre (Robarts Research Institute, London, Ontario) according to the manufacturer's protocols (Affymetrix, Santa Clara, CA). $N = 3$ biologic replicates for the higher *versus* lower Daoy MB tumor spheres were analyzed. Ten micrograms of cRNA was labeled and hybridized to the Affymetrix Human Gene 1.0 ST chips. Expression signals were scanned on an Affymetrix GeneChip Scanner and data extraction was performed using Affymetrix AGCC software. Data normalization and analysis was performed using Dchip software. Hierarchical clustering using Pearson correlation coefficients was performed on the normalized data. Differentially expressed genes were analyzed using Ingenuity Pathway Analysis (Redwood City, CA). Transcripts dysregulated at least two-fold (upregulated or downregulated) in the higher *versus* lower self-renewing Daoy tumor spheres with a $P < .05$ were considered significant.

Exon Array Profiling

Affymetrix Human 1.0 exon array profiling was used to examine expression of CD271 (p75/NTR) in 14 normal cerebellar samples

(9 fetal and 5 adult) and 111 primary MBs [30]. Expression of CD271 (p75/NGFR) across all samples is presented in boxplot format as $\log_2$-transformed signal intensity.

Statistical Analysis

All tests were performed using Prism 5 software (GraphPad Software, La Jolla, CA) or SPSS Statistics (IBM, Armonk, NY). Descriptive statistics were used to determine significant differences including mean and SEM along with one-way analyses of variance, independent sample two-tailed *t* tests, and Tukey's test for multiple comparisons. *P* values less than .05 were considered significant.

Results

MB Subclones Exhibit Variable Morphology, Invasiveness, and Self-Renewal Capacity

To evaluate MB cellular heterogeneity, we first derived subclones from the Daoy MB cell line. Adherent Daoy cultures were dissociated

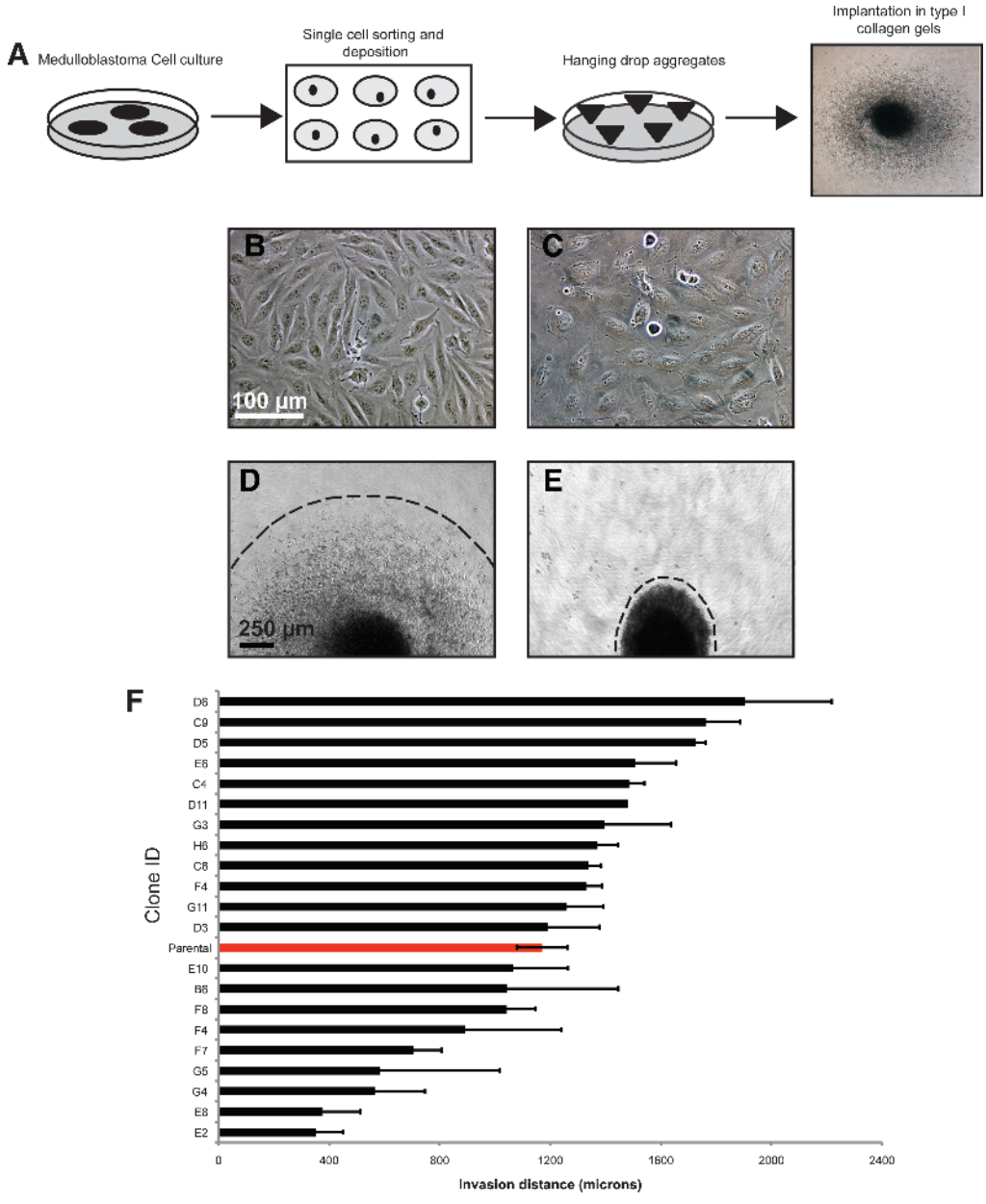

Figure 1. Subclones derived from Daoy MB cells exhibit morphologic and cellular heterogeneity. (A) Schematic depicting single-cell derived clonal expansion of Daoy cells after sorting. Expanded clones were cultured as hanging drop aggregates for 3 days and then placed into three-dimensional type I collagen gels to follow invasion for 72 hours. (B–E) Representative images of monolayer adherent cultures and hanging drop aggregates from Daoy subclones. Note that some clones exhibited an elongated morphology (B) and others displayed a rounded or ruffled (C) appearance. Scale bar, 100 μm. When placed in collagen gels, hanging drops from elongated clones exhibited a higher invasive capacity (D), whereas hanging drops derived from rounded clones typically grew in collagen but only minimally invaded (E). Scale bar, 250 μm. (F) Invasive capacity of all 21 subclones derived from the parental Daoy MB cell line. Error bars, SEM.

into a single-cell suspension and single cells were sorted and individually plates (Figure 1*A*). A expanded and then cultured aggregate preparation [29] (Figure 1, *A–C*). Aggregate spheroids were implanted into collagen gels, and invasion was measured after 72 hours (Figure 1, *A*, *D*, and *E*). The 21 subclones exhibited morphologic heterogeneity with some displaying an elongated appearance (Figure 1*B*), while others exhibit a rounded or ruffled morphology (Figure 1*C*). The elongated subclones demonstrated a higher invasive capacity than the rounded clones (Figure 1, *D* and *E*). In addition, there was a six-fold invasion difference between the clones exhibiting the highest and least invasive capacity (Figure 1*F*). The most (N = 5 independent subclones) and least (N = 3 independent subclones) invasive subclones were then plated into neural stem cell (NSC) culture at a concentration of 20,000 cells/well (5 cells/μl) to examine self-renewal. In bulk culture, tumor spheres derived from the most invasive subclones exhibited a significantly higher self-renewal capacity when placed in NSC culture, spheres and this passages (Figure 2*A*). After invasive subclones began subsequently expanded as adherent cultures (Figure 2, *B* and *C*). Tumor spheres from the most invasive subclones did not adhere and continued to maintain their self-renewal capacity. Together, these results demonstrate that MB cultures exhibit morphologic and cellular heterogeneity. Although subcloning leads to independent, phenotypically distinct subcultures of Daoy cells, there are likely still subpopulations or lineages of cells within each of these clonally derived lines that could separately account for the self-renewing and invasive behaviors. To further define these subpopulations, we must perform expression profiling to determine which cell surface markers may select for highly self-renewing or invasive phenotypes.

Tumor Spheres Displaying Higher versus *Lower Self-Renewal Capacity Exhibit Differential Expression of CD271*

Tumor spheres derived from our MB subclones displayed differential self-renewal capacity. Therefore, we wanted to test whether these same tumor spheres also exhibit changes in cell surface marker expression. Passage 1 tumor spheres from subclones displaying higher self-renewal (N = 5 independent subclones) *versus* lower self-renewal (N = 3 independent subclones) were comparatively screened for the presence of cell surface markers already known to play a role in neural lineage specification, BTPCs, and/or tumor cell metastasis (Figure 2, *D–L*). Comparative analysis of higher *versus* lower self-renewing tumor spheres using flow cytometry revealed significant differential expression of CD271 (p75NTR; Figure 2*I*). CD24 and CD133 also showed differential expression; however, the results were not significant (Figure 2, *J* and *L*). Breakdown of higher *versus* lower self-renewing tumor spheres into individual subclones revealed that four of five highly self-renewing subclones tested exhibited elevated levels of CD271, whereas all three lower self-renewing subclones tested expressed very low levels (Figure 2*M*). To assess whether CD271, CD133, and CD24 are enriched in tumor sphere culture, we examined expression levels in confluent adherent cultures with 10% FBS relative to passage 1 and passage 2 tumor spheres (Figure 2, *N* and *O*). CD271 and CD133 are elevated following enrichment for the stem cell–like phenotype (Figure 2*N*). In fact, CD271 levels are enriched 77-fold, even higher than the 36-fold enrichment seen with CD133 (Figure 2*N*). In contrast, CD24 exhibits a rapid decline over subsequent tumor sphere passages (Figure 2*O*). To determine whether CD271 and CD133 are also enriched in other MB cell lines, we examined expression levels in adherent *versus* tumor sphere culture from D283 MB cells. Compared to adherent cultures, D283 tumor spheres exhibit a small but significant and consistent increase in CD271 expression (Figure W1*A*). Interestingly, CD133 levels declined following culture of D283 cells as tumor spheres (Figure W1*B*). We also examined CD271 and CD133 levels in our recently described transformed neural precursor model of MB [27]. Relative to normal human embryonic neural precursors (hENs), neoplastic or transformed human embryonic neural precursors (t-hENs), exhibit a higher self-renewal capacity *in vitro* and an MB phenotype *in vivo*. A comparison of t-hEN *versus* hEN cultures revealed a significant increase in CD271 levels in t-hEN MB–like cells (Figure W1*C*). CD133 levels exhibited wide variation between trials and overall remain unchanged (Figure W1*D*). Together, these results demonstrate that CD133 patterns vary between cell lines and support recent findings suggesting that CD133 should not be used as an exclusive marker for selection of BTPCs [8–12]. Interestingly, in the cell lines tested, CD271 is consistently higher in tumor sphere culture or MB cells with a higher self-renewal capacity. CD271 may therefore play a novel role in selecting for MB TPCs *in vitro*.

Migrating MB Cells Exhibit Decreased CD271/CD24 and Increased CD133 Expression

Tumor spheres derived from the higher *versus* lower self-renewing MB subclones exhibit differential expression of CD271. These results may be attributed to the differences in self-renewal between subclones specifically in tumor sphere culture or may be linked to the differential invasive capacities of the parental cultures when placed in collagen gels. It is unclear whether changing the biologic context will also change the expression patterns of these cell surface markers. To test the possibility that cell surface markers exhibit differential expression

Figure 2. Self-renewal capacity and expression of CD271 differs in MB tumor sphere subclones. (A) Self-renewal capacity of the most *versus* the least invasive derived tumor spheres. In NSC culture, the most invasive subclones gave rise to a higher number of tumor spheres over two passages indicative of a higher self-renewal capacity. Error bars, SEM; $^{**}P < .01$; $N = 3$ independent experiments. (B, C) Bright-field images of higher (B) *versus* lower (C) self-renewing tumor spheres after three passages in culture conditions enriching for BTPC populations. Scale bar, 200 μm. (D) Schematic depicting the procedure used for comparative cell surface marker expression. MB subclones were placed in NSC culture, and tumor spheres exhibiting higher *versus* lower self-renewal capacity (SR) were comparatively screened for the presence of cell surface markers. (E–L) Quantification of cell surface marker screen on the higher *versus* lower self-renewing (SR) MB tumor spheres. Error bars, SEM; $^{*}P < .05$; $N = 5$ independent "higher self-renewing" subclones, $N = 3$ independent "lower self-renewing" subclones. Each subclone was screened between one and four times, and results were pooled. (M) Breakdown of the higher *versus* lower self-renewing tumor sphere subclones for CD271. Four of five higher self-renewing subclones expressed CD271, while zero of three lower self-renewing subclones expressed significant levels of CD271. (N) Daoy parental adherent cultures grown in 10% FBS exhibit low CD271 and CD133 expression by flow cytometry (left panel). Daoy tumor spheres (passage 1, middle panel; passage 2, right panel) grown in BTPC conditions exhibit an enrichment of CD271 and CD133 expression by flow cytometry relative to adherent cultures. Insets: live cell–only controls. (O) Down-regulation of CD24 expression following culture of MB adherent cultures in NSC conditions.

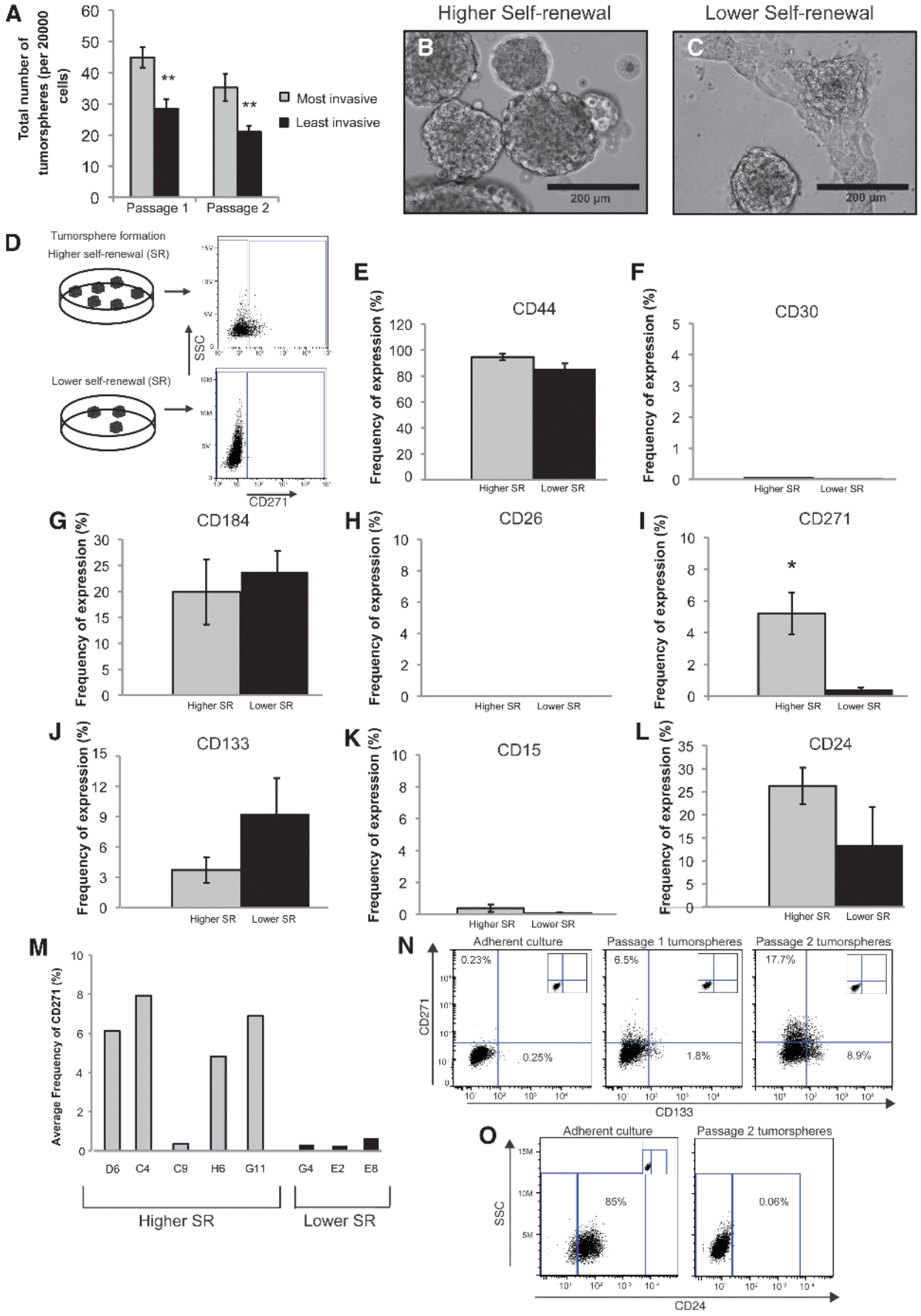
A
Total number of tumorspheres (per 20000 cells)
Most invasive
Least invasive
Passage 1
Passage 2
Higher Self-renewal
Lower Self-renewal
B
C
200 µm
D
Tumorsphere formation
Higher self-renewal (SR)
Lower self-renewal (SR)
SSC
CD271
E
CD44
F
CD30
G
CD184
H
CD26
I
CD271
J
CD133
K
CD15
L
CD24
Frequency of expression (%)
Higher SR
Lower SR
M
Average Frequency of CD271 (%)
D6
C4
C9
H6
G11
G4
E2
E8
N
Adherent culture
Passage 1 tumorspheres
Passage 2 tumorspheres
0.23%
0.25%
6.5%
1.8%
17.7%
8.9%
CD271
CD133
O
Adherent culture
Passage 2 tumorspheres
85%
0.06%
SSC
CD24

patterns in other biologic assays, we conducted aggregates to separate the stationary cells (Figure 3, *A* and *B*). MB hanging drop aggregates from the parental Daoy cell line were allowed to adhere to a cell culture plate surface and individual cells migrated out from the center over a 48-hour period. The aggregate core was mechanically dissected and both "core" and "migrating" cell populations were dissociated and subjected to our eight-cell surface marker antibody screen. CD271 was significantly different between core and migrating cell populations. In these cell conditions, CD24 and CD133 were also significantly different (Figure 3, *C–J*). Interestingly, CD271/CD24 levels were higher in the core cell population, whereas CD133 was higher in the migrating cells (Figure 3, *C–J*). In addition, we examined transcript levels of neural lineage markers by qPCR and found that the primitive neuroectoderm marker Otx2 was significantly higher in the core cell population, while Sox1 levels remain unchanged (Figure 3*K*). Interestingly, the more differentiated βIII tubulin was significantly lower in this core population (Figure 3*K*). This was supported at the protein level by flow cytometry studies demonstrating lower βIII tubulin in the core population (data not shown). However, nestin levels were not significantly different (data not shown). Taken together, these results demonstrate that lower CD271/CD24 and higher CD133 levels "mark" a migrating MB *versus* a core cell and that migrating MB cells may represent a slightly more differentiated state. Differential expression patterns in the tumor spheres (Figure 2) may therefore reflect changes in self-renewal capacity between the MB subclones. These seemingly opposing results can be explained by the biologic context or cellular conditions the MB cells are subjected to. Our results point to novel functional relationships among cells expressing CD271, CD24, and CD133. However, as CD271 was significantly and consistently elevated in higher self-renewing tumor spheres and CD133 has been widely implicated in brain tumorigenesis, we chose to further pursue the relationship between CD271 and CD133 for additional experiments.

CD271 Selects for MB Cells with Increased Self-Renewal while CD133 Selects for Cells Exhibiting Higher Invasion

From our screening data, we predicted that CD271 and CD133 would mark cells displaying differences in cellular properties. To test this hypothesis, we used fluorescence-activated cell sorting tumor spheres based CD271 Figure 4, these experiments, procedure than D283, hEN, and t-hEN cell lines. Purified subpopulations were then subjected to tumor sphere assays, cumulative cell counts in adherent culture, and invasion assays in collagen gels (Figure 4*A*).

Sorted MB cells from tumor spheres were replated in NSC culture at a density of 2500 cells/well (2.5 cells/μl) and the number of tumor spheres was counted after 5 days (Figure 4, *C* and *D*). Cell populations positive for CD271 (CD133–/CD271+ and CD133+/CD271+) generated a higher number of tumor spheres over passage (Figure 4, *C* and *D*). CD133–/CD271+ cells displayed the highest enrichment of tumor spheres with a more than three-fold increase in tumor sphere number from passages 1 to 2. Our results demonstrate that CD271 select for MB cells with the highest self-renewal capacity *in vitro*. These data are consistent with our findings that both CD271 and CD133 are elevated in stem cell culture (Figure 2*N*); however, CD271, with an even higher enrichment in Daoy cells, may better select for MB-propagating cells *in vitro*.

Sorted subpopulations from MB tumor spheres were also subjected to cell count assays. Briefly, 2500 cells from sorted populations were plated in adherent conditions in media containing 10% FBS, and cumulative cell counts were taken after 4 days. Our results demonstrate that the CD133–/CD271– population exhibits a significantly higher number of cells after 4 days (Figure 4*E*). Interestingly, the other three subpopulations exhibit a total cell number lower than the starting cell population, suggesting a possible survival effect in adherent culture. These results demonstrate that the fractions exhibiting an elevated capacity for self-renewal are not the same as those with the highest cumulative cell number overtime.

In contrast to our results for self-renewal, when sorted MB subpopulations were cultured as hanging drop aggregates and then placed into collagen gel invasion assays, the CD133+/CD271– subpopulation demonstrated a higher invasive capacity (Figure 4, *F* and *G*). Invasion was always highest in the MB subpopulations that exhibit a lower self-renewal capacity. In addition, we noted a distinct invasion pattern between the CD133+/CD271– and CD133–/CD271– cells with the former invading as a collective wave of cells, whereas the latter is characterized by leading elongated cells and a stream of less invasive cells lagging behind (Figure 4*F*). While the invasion increase in CD133+/CD271– cells was not significantly different from the other subpopulations, it should be noted that we were often unable to obtain high CD133+ cell numbers and, consequently, were only able to generate two complete data sets with replicates from all four subpopulations. However, these trends support our core *versus* migrating cell data (Figure 3), where CD271 levels are higher in the core cells and CD133 expression is elevated in migrating cells. Collectively, our data demonstrate that combinatory expression of CD271 and CD133 enables selection for MB cells displaying variations in cellular properties.

CD271+ MB Cells Exhibit Chemoresistance at Low Concentrations

It is well documented that both BTPCs and highly invasive cells are resistant to conventional therapies such as chemotherapy and radiation [16–22]. However, the majority of these studies were conducted in GBM models, and less is known about the effect of therapeutic treatments on putative MB self-renewing cells. To investigate the effect of chemotherapeutic agents on MB subpopulations treated MB tumor days Figure 5, A and increased apoptosis enrichment of the CD133–/CD271+ subpopulation at the lowest concentration of 5-FU (Figure 5, *M–Q*). After 14 days, the CD133–/CD271+ fraction that exhibits a higher capacity for self-renewal is nearly doubled (Figure 5*Q*). At higher concentrations, the CD133–/CD271+ subpopulation is significantly decreased but is still present after 14 days (Figure 5, *O–Q*). These patterns are also sustained after 21 days of treatment (data not shown). Taken together, these results demonstrate that chemotherapeutic agents fail to eliminate the cell population with the highest capacity for self-renewal and suggest that in our MB model system, the CD133–/CD271+ may represent a drug-resistant phenotype.

CD133–/CD271+ Cells Exhibit Tumor-Initiating Capacity In Vivo

We have shown that CD271 has a novel role in selecting for highly self-renewing MB cells *in vitro*. We hypothesized that these cells would also exhibit tumor-initiating capacity *in vivo*. To test this, we specifically sorted CD133–/CD271+ and CD133–/CD271– cells from MB tumor spheres and injected 2×10^5 cells for each subpopulation ($N = 3$ CD133–/CD271+ and $N = 4$ CD133–/CD271–) along with unsorted cells from MB tumor spheres ($N = 4$) intracranially into mice. After 5 weeks (36 ± 1 days), animals injected with CD133–/CD271+

cells started to exhibit neurologic signs of potential tumor head (Figure 6*A*). While unsorted tumor sphere cells also exhibited these neurologic signs, this was typically delayed. The average time between injection and neurologic signs was 41 ± 2.5 days for CD133–/CD271– cells and 44 ± 2 days for unsorted MB tumor sphere cells (Figure 6*A*). After 7.5 weeks, mice injected with unsorted MB tumor spheres displayed rare clusters of malignant cells typically confined to the subarachnoid space (Figure 6, *C* and *F*). However, mice injected with

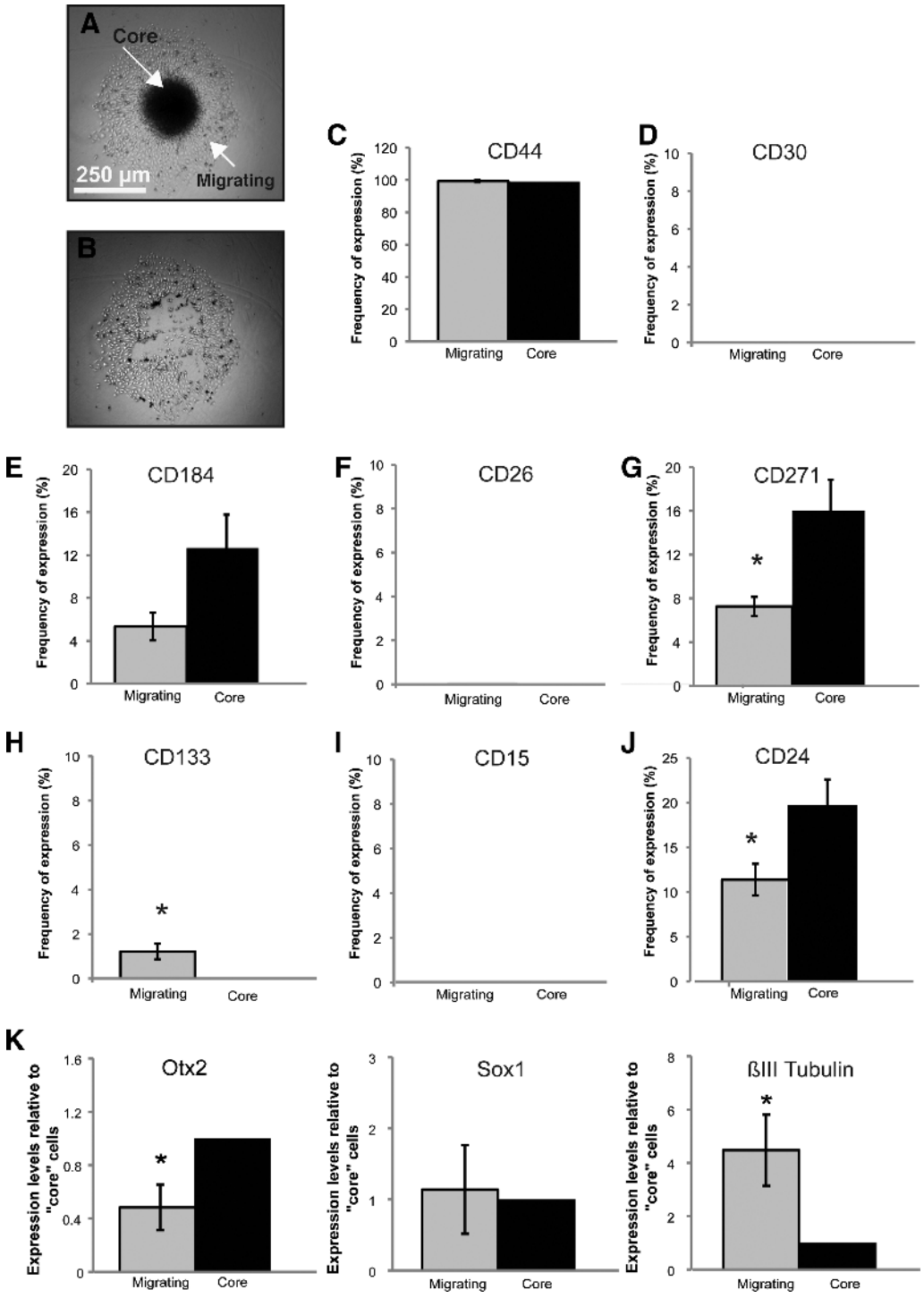

Figure 3. Comparative cell surface marker expression from "core" *versus* "migrating" MB cells reveals differential expression of CD271, CD133, and CD24. (A, B) Images of an MB hanging drop aggregate before (A) and after (B) manual "core" dissection. Scale bar, 250 µm. (C–J) Cell surface marker antibody screen on the "core" *versus* "migrating" cells from MB aggregates 48 hours after attachment. Cell surface markers were chosen on the basis of their proposed role in neural lineage specification, brain tumor stem cell self-renewal, and tumor cell invasion. Error bars, SEM; *$P < .05$; $N = 4$ and $N = 3$ independent experiments. (K) qPCR analysis of selected neural stem cell/primitive neural transcripts and differentiated neuronal markers in "core" *versus* "migrating" Daoy MB cells. Error bars, SEM; *$P < .05$.

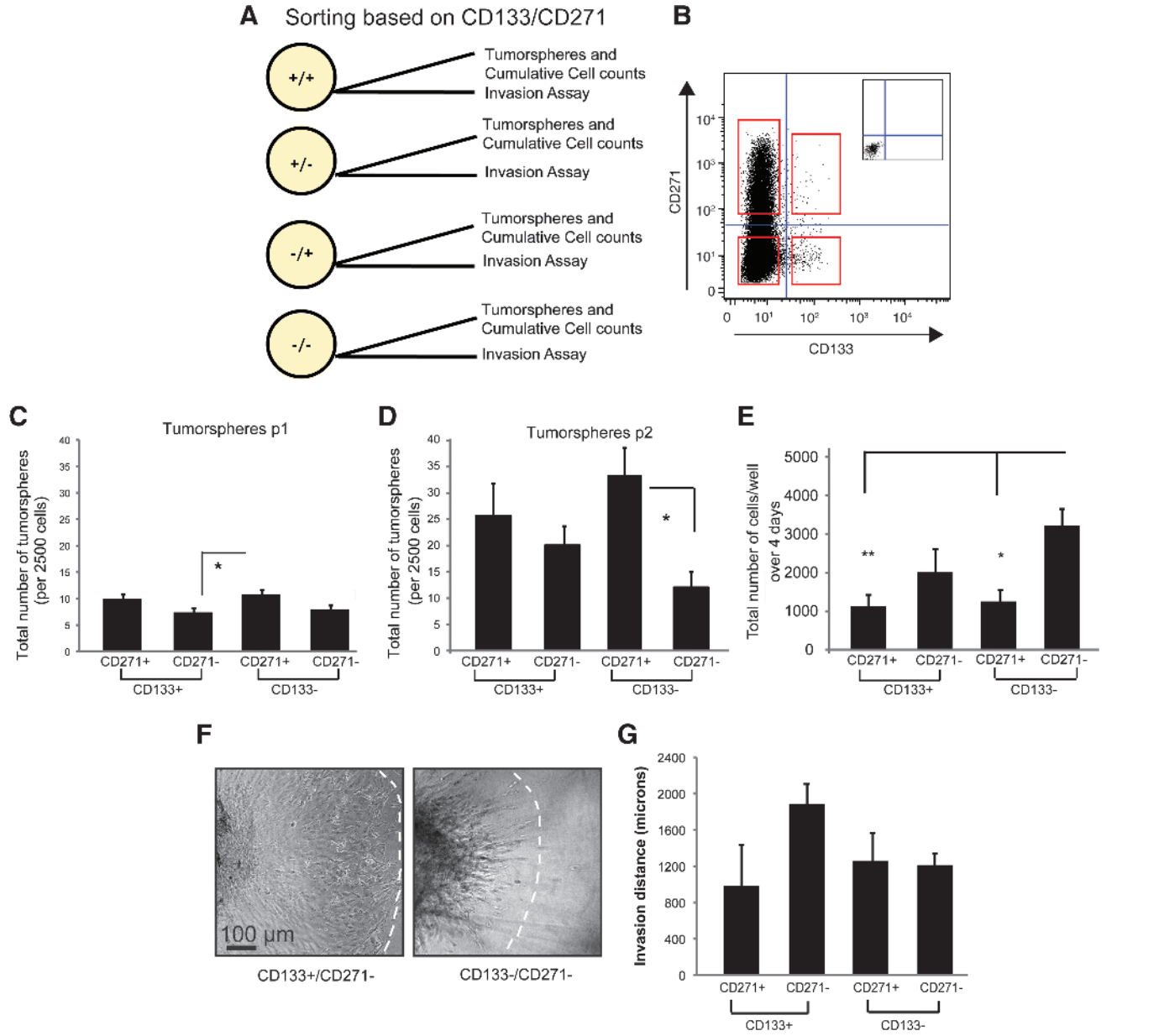

Figure 4. CD271 selects for cells exhibiting higher self-renewal capacity and CD133 selects for cells demonstrating higher invasion. (A) Schematic depicting initial two-marker sorting strategy to obtain four subpopulations. (B) Representative dot plot of sorting paradigm used to select cells based on CD133/CD271 expression. Red squares depict cell populations from all four quadrants to be sorted. (C, D) Tumor sphere assays for MB subpopulations following FACS. (C) Tumor spheres sorted on CD133/CD271 at the first passage (p1) following FACS; $N = 3$ independent experiments. (D) Tumor spheres sorted on CD133/CD271 at the second passage (p2) following FACS. Error bars, SEM; $^*P < .05$. (E) Average total number of cells/well in adherent culture following FACS. Error bars, SEM; $^*P < .05$, $^{**}P < .01$; $N = 3$ independent experiments. (F, G) Invasion assays from subpopulations sorted on CD133/CD271. (F) Representative images of the highly invasive CD133+/CD271− subpopulation and the less invasive CD133−/CD271− subpopulation after 3 days in collagen gels. Scale bar, 100 μm. (G) Quantification of invasion for each subpopulation after 3 days in collagen following CD133/CD271 sorts. Error bars, SEM; $N = 2$ independent experiments.

CD133−/CD271+ cells displayed the most prominent tumorigenic features (Figure 6, *B*, *D*, and*G*), characterized by a dense mass of malignant cells exhibiting a high nuclear-to-cytoplasmic ratio, abundant mitotic and apoptotic figures, diffuse infiltration of malignant cells in the subarachnoid compartment at the base of the brain, and intense infiltration into the brain along perivascular spaces (Figure 6, *B*, *D*, and *G*). This was associated with hydrocephalus due to obstructed cerebrospinal fluid flow. Mice injected with CD133−/CD271− cells also displayed tumorigenic features (Figure 6, *B*, *E*, and *H*); however, infiltration along perivascular spaces was minimal in comparison (Figure 6, *E* and *H*). Together, these results demonstrate that CD271+ cells exhibit the capacity for tumor initiation *in vivo*.

The ability of both CD133−/CD271+ and CD133−/CD271− cells to initiate tumor formation may reflect 1) each individual sorted subpopulation's capacity for tumor initiation or 2) a subpopulation's ability to reestablish heterogeneity and all cell phenotypes following

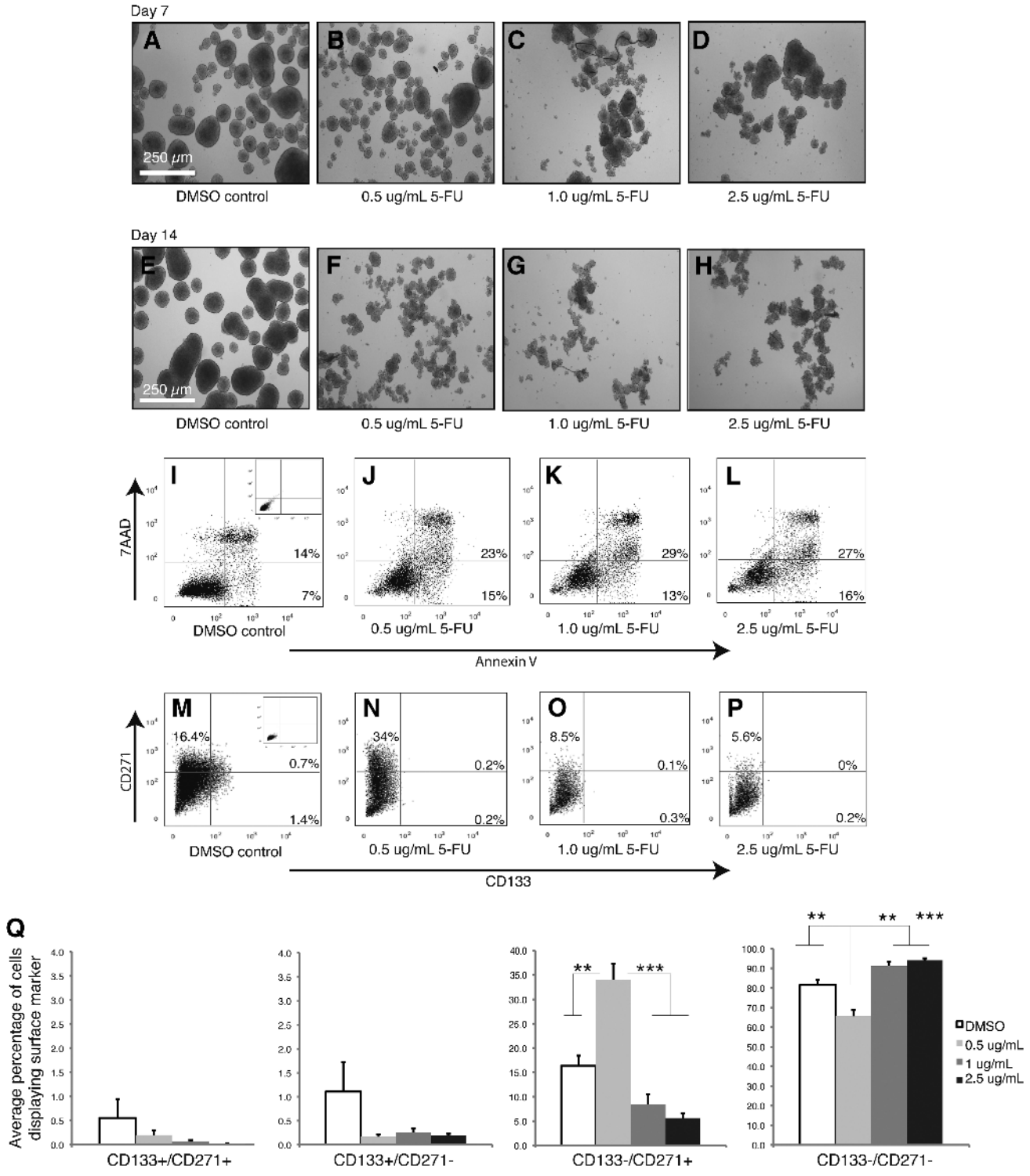

Figure 5. 5-FU treatment of MB tumor spheres leads to an enrichment of the CD133−/CD271+ subpopulation. (A–H) Representative images of Daoy MB tumor spheres treated with 0.5, 1.0, and 2.5 μg/ml 5-FU relative to DMSO controls after 7 days (A–D) and 14 days (E–H). Scale bar, 250 μm. (I–L) Annexin V/7AAD analysis of Daoy MB tumor spheres treated with 0.5, 1.0, and 2.5 μg/ml 5-FU relative to DMSO controls after 14 days. (M–Q) Quantification of the effect of 5-FU on CD133/CD271 subpopulations after 14 days. (M–P) Representative flow cytometry images of CD133/CD271 expression following treatment with DMSO and 0.5, 1.0, and 2.5 μg/ml 5-FU. (Q) Quantification of the frequency of specific CD133/CD271 subpopulations following treatment with 5-FU. Error bars, SEM; $^{**}P < .01$, $^{***}P < .001$; $N = 4$ independent experiments.

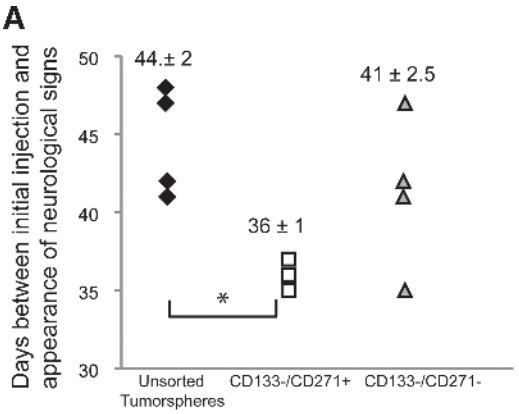
A
Days between initial injection and appearance of neurological signs
50
45
40
35
30
44.± 2
36 ± 1
41 ± 2.5
*
Unsorted Tumorspheres
CD133-/CD271+
CD133-/CD271-

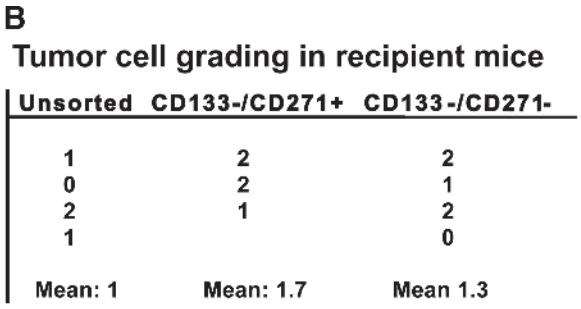
B
Tumor cell grading in recipient mice
Unsorted
1
0
2
1
Mean: 1
CD133-/CD271+
2
2
1
Mean: 1.7
CD133-/CD271-
2
1
2
0
Mean 1.3

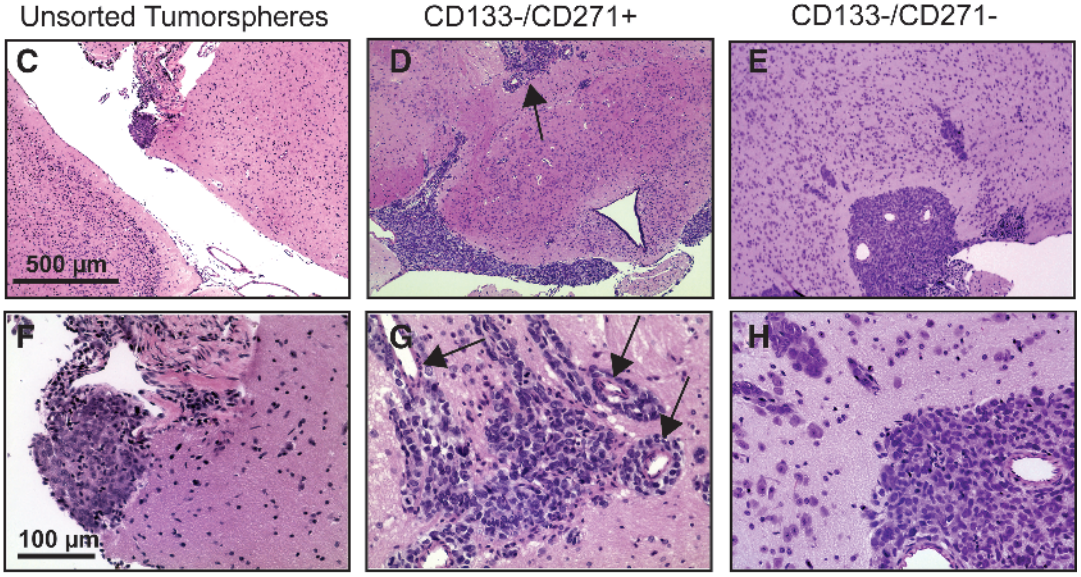
Unsorted Tumorspheres
CD133-/CD271+
CD133-/CD271-
C
D
E
500 µm
F
G
H
100 µm

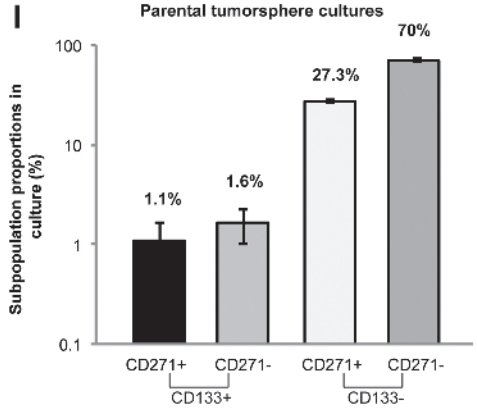
I
Parental tumorsphere cultures
Subpopulation proportions in culture (%)
100
10
1
0.1
1.1%
1.6%
27.3%
70%
CD271+
CD271-
CD271+
CD271-
CD133+
CD133-

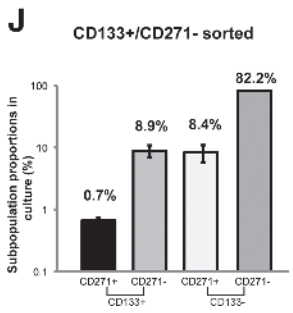
J
CD133+/CD271- sorted
Subpopulation proportions in culture (%)
0.7%
8.9%
8.4%
82.2%

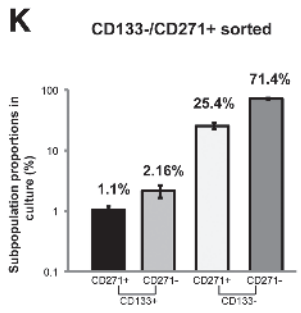
K
CD133-/CD271+ sorted
Subpopulation proportions in culture (%)
1.1%
2.16%
25.4%
71.4%

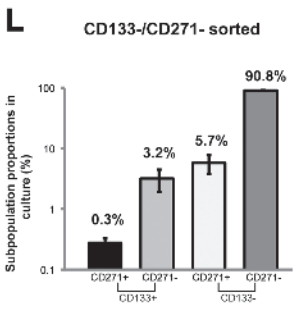
L
CD133-/CD271- sorted
Subpopulation proportions in culture (%)
0.3%
3.2%
5.7%
90.8%

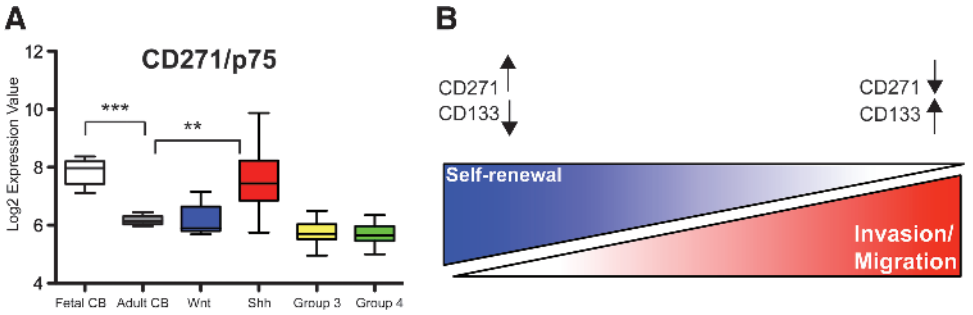

Figure 7. CD271 levels are highest in fetal cerebellum and Shh MB and lower in more invasive and aggressive group 3 and group 4 molecular variants. (A) Data from Affymetrix exon array profiling of 14 normal cerebellar (9 fetal and 5 adult) samples (CB) and 111 primary MB presented as boxplots. CD271 expression is significantly higher in the fetal CB (***$P < .001$) and Shh subgroup (**$P < .01$) relative to the more differentiated adult cerebellar samples and significantly lower in groups 3 (*$P < .05$) and 4 (**$P < .01$). Bars denote 1.5 interquartile range within each group. (B) Working model depicting spectrum of cellular phenotypes and novel functional relationships among cells expressing CD271 and CD133.

intracranial transplantation. To test these hypotheses, we recultured 1 × 10^4 sorted CD133+/CD271−, CD133−/CD271+, and CD133−/CD271− cells as tumor spheres and analyzed CD271 and CD133 levels after 6 days. CD133−/CD271+ cells consistently recapitulated the distribution of parental tumor sphere culture phenotypes (Figure 6, *I–L*). In particular, the >10:1 ratio of CD133−/CD271+ to CD133+/CD271− cells was maintained. Both CD133+/CD271− and CD133−/CD271− cells were also able to generate all four subpopulations, albeit at different ratios with a notable decline in CD271 (Figure 6, *I–L*). Together, these results demonstrate that sorted subpopulations reset phenotypic equilibrium in culture. This reestablishment could lead to tumor initiation from the different subpopulations *in vivo*. Our data support the idea that cell subpopulations can transition between higher self-renewing and invasive states.

CD271 Levels Are Higher in the Shh MB Molecular Variant and Fetal Cerebellum and Lowest in the More Aggressive, Invasive Group 3 and 4 Subgroups

Recent studies have demonstrated that MB is divided into distinct molecular subtypes [31]. In particular, a Wnt pathway variant, a Shh pathway variant, and highly aggressive, metastatic group 3 and 4 subgroups have been identified [30,31]. On the basis of the expression patterns of CD271 *in vitro*, we predicted that CD271 levels would be higher in the typically less aggressive Shh and Wnt variants relative to the invasive/metastatic group 3 and 4 subgroups. To test this hypothesis, we probed for expression of CD271 in an MB data set derived from exon array profiling of 111 primary MB and 14 normal human cerebellar samples (9 fetal cerebellum and 5 adult cerebellum). CD271 expression was significantly higher in fetal cerebellum and the Shh molecular variant cerebellum (Figure 7*A*). As and 4 (Figure 7*A*). While CD271 expression in the Wnt subgroup was higher than in groups 3 and 4, the levels were not significantly different. Overall, these results lend further support to the concept that CD271 levels are lower in the most invasive/metastatic phenotypes.

Highly Self-Renewing MB Tumor Spheres Exhibit Down-Regulation of the Cell Motility Transcription Program

Our screening and sorting results demonstrate CD271↑, CD133↓ in highly self-renewing tumor spheres but CD271↓, CD133↑ in migrating/invading cells. Even though the higher self-renewing tumor sphere subclones were derived from adherent cultures exhibiting elevated invasion in collagen gel assays, it is unclear whether cells in the "stem cell" or tumor sphere microenvironment exhibit the same capacity for cell motility. To address this, we conducted global gene expression analysis on higher *versus* lower self-renewing MB tumor spheres from independent subclones. Affymetrix analysis revealed that a total of 264 transcripts were significantly and differentially expressed between the higher *versus* lower self-renewing MB tumor spheres (Table W1). Eighty-four transcripts were associated with cellular movement, of which 67 (80%) were downregulated (Figure W2 and Table W2). On the basis of the directional changes and known function of the associated transcripts, cellular movement was predicted to be decreased in higher self-renewing tumor spheres (Table W3). Among the cellular movement transcripts, pathways (Table 1). In B signaling pathways, including the receptors EPHB1, EPHB3, and EPHB6 as well as the ligand ephrin B2 (Table 1).

Figure 6. CD133−/CD271+ cells exhibit tumor-initiating cell capacity *in vivo* and MB subpopulations can reestablish phenotypic heterogeneity following reculture as tumor spheres. (A) Scatterplot depicting time between injections of unsorted or sorted MB tumor sphere subpopulations and signs of tumor formation including appearance of a domed head caused by hydrocephalus. *$P < .05$. (B) Semiquantitative scoring of Daoy MB tumor samples, based on a scale of 0 to 3, where 0 = no malignant cells, 1 = rare clusters of malignant cells confined to the subarachnoid space, 2 = malignant cells in subarachnoid compartment and invasion along perivascular spaces, 3 = features in 2 plus tumor nodules growing in other areas of the brain or cerebellum. (C–H) Infiltration of malignant MB cells from unsorted tumor spheres (C, F), CD133−/CD271+ cells (D, G), and CD133−/CD271− cells (E, H). Arrows in the upper panels depict highly infiltrative MB cells and formation of smaller clusters of MB cells throughout the brain. The arrows in the lower panel denote intense perivascular infiltration. Scale bars, 500 μm (upper panels), 100 μm (lower panels). (I–L) Parental Daoy MB tumor spheres (I) were sorted on the basis of CD133/CD271 expression. Three subpopulations were sorted and recultured as tumor spheres for 6 days (J–L). Cultures derived from sorted subpopulations were then evaluated for CD133/CD271 expression. Error bars, SEM.

Table 1. Dysregulation of Neural Developmental Pathway Transcripts in the Higher *versus* Lower Self-Renewing MB Tumor Spheres.

Entrez Gene Name	Affymetrix/Entrez Gene/ Gene Symbol	Fold change (Higher *versus* Lower Self-Renewing Tumor Spheres)
Myosin, light chain 1, alkali; skeletal, fast	MYL1	4.2751
p21 protein (Cdc42/Rac)–activated kinase 3	PAK3	2.61359
Neurotrophic tyrosine kinase, receptor, type 2	NTRK2	2.44057
EPH receptor B1	**EPHB1**	**2.16958**
Myosin light chain, phosphorylatable, fast skeletal muscle	MYLPF	2.14949
EPH receptor B3	**EPHB3**	**2.11716**
Dihydropyrimidinase-like 5	DPYSL5	2.06395
Tubulin, β4	TUBB4	2.02616
EPH receptor B6	**EPHB6**	**–2.05668**
Patched 2	PTCH2	–2.12875
Slit homolog 3 (Drosophila)	SLIT3	–2.57108
Ephrin-B2	**EFNB2**	**–2.69877**
Sema domain, immunoglobulin domain (Ig), short basic domain, secreted, (semaphorin) 3C	SEMA3C	–2.8071
Sema domain, seven thrombospondin repeats (type 1 and type 1–like), transmembrane domain (TM) and short cytoplasmic domain, (semaphorin) 5A	SEMA5A	–3.1147

Eph-ephrin signaling transcripts are in **bold**.

These results demonstrate that there is an overall down-regulation of a cell motility program in higher self-renewing MB tumor spheres and that dysregulated Eph-ephrin signaling may be involved in MB TPC function.

We have demonstrated differential expression of Eph-ephrin pathway ligands and receptors in the higher *versus* lower self-renewing tumor spheres; therefore, we also wanted to see whether this pathway is also dysregulated in MB core *versus* migrating cells. We examined transcript levels of the ephrin B2 ligand as well as the receptors EPHB1, B2, B3, B4, and B6 by qPCR. We found that the ligand ephrin B2 as well as the receptors EPHB1 and EPHB2 are significantly upregulated in the migrating *versus* the core cells, while the receptors EPHB3 and B4 are significantly downregulated (Figure W3, *A*–*F*). Together, our results demonstrate that the Eph-ephrin pathway is not only differentially expressed in tumor spheres with variable self-renewal capacity but also in migrating *versus* core MB cells. These data suggest that the Eph-ephrin pathway may play an important functional role in both MB TPCs and migration/invasion.

Discussion

In this study, we deconstructed MB cellular heterogeneity and identified a novel role for CD271 in enriching for a highly self-renewing MB phenotype. We propose a dynamic model (Figure 7*B*) whereby a highly self-renewing CD271↑, CD133↓ cell in the MB tumor core may help sustain tumorigenesis. Once a cell commits its metabolic machinery to migration and/or invasion, the levels of these cell surface markers change, and a highly motile cell will acquire a CD271↓, CD133↑ signature. As self-renewal and invasion are not mutually exclusive, this concept aligns with recent studies demonstrating that both CD133+ and CD133– cells exhibit BTPC function [8,9,11]. In addition, our work is also consistent with findings in glioblastoma that reveal a spectrum of self-renewing and aggressive cellular phenotypes that differentially express CD133 [12]. Highly self-renewing and invasive cells have also been shown to proliferate less. Therefore, it is not surprising that these subpopulations are distinct from those exhibiting the highest cumulative cell count in our study. However, it should be noted that the higher total cell number observed in CD133/–CD271– MB cells might be attributed to a variety of mechanisms including increased adhesion and/or survival upon replating of sorted subpopulations combined with possible differences in cell cycle properties. While we also observed some interesting trends with CD24, this cell surface marker was in fact downregulated in stem cell conditions relative to adherent cultures. This suggests that CD24 may mark an MB progenitor population and is supported by expression patterns during neural lineage specification where high levels of CD24 are observed in transit-amplifying cells [32] and differentiated neurons [33] and lower expression is seen in NSCs [34,35].

The inverse but not mutually exclusive correlation between self-renewal and invasion is seemingly at odds with the positive relationship between our most highly invasive MB subclones and their self-renewal capacity depicted in Figure 2, *A* to *C*. These experiments were conducted in bulk culture and did not determine whether those cells that are invading are the same self-renewing TPCs that ultimately sustain tumor sphere cultures. In fact, molecular characterization of the highly self-renewing *versus* lower self-renewing tumor spheres from independent subclones revealed a global down-regulation of the cell motility transcription program in highly self-renewing tumor spheres. Even though the higher self-renewing tumor spheres were derived from adherent cultures exhibiting elevated invasion in collagen gel assays, when placed in tumor sphere culture, the cell movement program is downregulated. Therefore, changing the biologic context or microenvironment also changes gene expression patterns representative of a particular cell state. This is supported by our screening results demonstrating CD271↑, CD133↓ in highly self-renewing tumor spheres but CD271↓, CD133↑ in migrating cells. Indeed, these cell subpopulations are not in a "static" state and can transition between phenotypes to reestablish cellular heterogeneity. This concept was recently demonstrated by Gupta et al. [15] with an elegant series of experiments using breast cancer cell lines. Therefore, we cannot assume that a particular set of cell surface markers will only select for one specific tumor cell phenotype. Future studies will examine the epigenetic mechanisms that may be responsible for the suppression of the cell motility program in higher self-renewing MB tumor spheres.

CD271 is commonly referred to as p75 or p75NTR and is a member of the tumor necrosis factor receptor family [36]. The receptor normally functions in the development of the nervous system, including growth cone elongation and axon guidance. CD271 has proapoptotic and prosurvival effects, depending on the neurotrophin ligand [36]. Recently, this receptor has also been linked to glioblastoma

invasion [37] and could be targeted with the use of γ-secretase inhibitors [38]. CD271 is also present in MB as well as the external granular layer (EGL) and Purkinje layer in the developing human cerebellum but absent in the adult cerebellum [39]. On the basis of expression in both human fetal cerebellum and MB patient samples, the authors suggested that CD271 could be a precursor marker linked with more primitive cell populations [39]. Our primary patient MB and cerebellar sample data revealed the same CD271 patterns. Interestingly, studies have also demonstrated that CD271-positive cells in the EGL are negative for CD133 [39]. This suggests that an inverse relationship between these cell surface markers may also exist in the developing cerebellum. It has been shown that granular neural precursors from the cerebellar EGL are the cell of origin for the Shh-MB variant [40,41]. The EGL is present in fetal but not adult cerebellum, and therefore, it is not surprising that fetal cerebellar and Shh tumor samples display high CD271 levels. CD271 may be important for Shh-driven or desmoplastic MB tumors. Recent work has demonstrated that CD271 is also involved with MB spinal metastasis [42]. While our study demonstrates that CD271+ cells do invade *in vitro*, they do not exhibit the highest invasive capacity. Future studies will explore the mechanisms responsible for the higher self-renewal capacity seen in CD271+ cells as well as a potential link between CD271 and Shh signaling in MB.

Another novel finding in our study was the differential expression of genes related to axon guidance in MB tumor spheres and core *versus* migrating cells. In particular, both ligands and receptors belonging to the EphB–ephrin B pathway were differentially expressed in MB tumor spheres as well as core *versus* migrating MB cells. Interestingly, global gene expression analysis on higher *versus* lower self-renewing glioblastoma tumor spheres also revealed differential expression of the same neurodevelopmental pathways, including six Eph-ephrin signaling ligand and receptors (unpublished data). These data support our MB findings and suggest that axon guidance pathways such as Eph-ephrin signaling play a functional role in malignant brain tumor–initiating cell or BTPC populations. The Eph-ephrin signaling pathways play important roles in cellular communication and regulate a variety of aspects during both normal development and disease progression including adhesion, migration, invasion, cell proliferation, survival, and cell morphology through reorganization of the actin cytoskeleton [43,44]. Notably, Eph-ephrin signaling has a well-established role in neurodevelopment [44] and recent studies have even demonstrated that ephrin signaling is regulated by CD271/p75NTR to control axon guidance and mapping [45,46]. This raises the intriguing possibility that Eph signaling and CD271 may be linked in MB as well. While studies have shown that the Eph-ephrin pathway plays an important role in glioma invasion [47–49] and most recently MB invasion *in vitro* [50], to our knowledge, this is the first study to evaluate the Eph-ephrin signaling expression profile in MB BTPC subpopulations. In fact, few studies have examined the functional role of axon guidance pathways specifically in MB [29]. These pathways may regulate the balance between MB self-renewal and invasion. Recent findings in glioblastoma lend support to this notion, as EphB2 signaling enhanced migration and invasion while decreasing cell proliferation from cells in tumor sphere culture [51].

In addition to Eph-ephrin signaling, our molecular profiling of higher *versus* lower self-renewing tumor sphere subclones also revealed differences in transcripts associated with the RhoGTPases such as p21 protein (Cdc42/Rac)–activated kinase 3. Although we did not specifically profile the sorted populations (i.e., CD133+/CD271− *versus* CD133−/CD271−) or the invading cells in our collagen assays, it is possible that the variation in cell motility patterns observed in these gels may also be attributed to differences in axon guidance pathways such as Eph-ephrin signaling and activation of RhoGTPases. Studies are currently underway to evaluate the functional significance of ephrin B–EphB signaling and the RhoGTPases in MB self-renewal *versus* invasion using our model system.

Combinatory expression of CD271 and CD133 may serve as important selective criteria for drug discovery that will enable concomitant targeting of a spectrum of putative MB-propagating cells and the most highly invasive cells that typically elude current therapies. We are currently pursuing higher throughput flow cytometry technologies to identify other potential cell surface markers that may also select for these transitory phenotypes. This will be important as our studies suggest that drugs targeting cells in the migratory or invasive state may not abrogate the putative TPCs in a state of higher self-renewal.

Acknowledgments

We thank Monroe Chan at the University of Manitoba Flow Cytometry Facility for technical support. We also thank Mark Nachtigal for critical review of the manuscript.

References

[1] Louis D, Ohgaki H, Wiestler OD, and Cavenee WK (2007). *WHO Classification of Tumours of the Central Nervous System* (4th ed). International Agency for Research on Cancer (IARC), Lyon, France.

[2] Mehta M, Chang S, Newton H, Guha A, and Vogelbaum M (2011). *Principles and Practice of Neuro-oncology: A Multidisciplinary Approach.* (1st ed). Demos Medical Publishing (Oct 21 2010), New York, NY.

[3] Wu X, Northcott PA, Dubuc A, Dupuy AJ, Shih DJ, Witt H, Croul S, Bouffet E, Fults DW, Eberhart CG, et al. (2012). Clonal selection drives genetic divergence of metastatic medulloblastoma. *Nature* **482**, 529–533.

[4] Rosen JM and Jordan CT (2009). The increasing complexity of the cancer stem cell paradigm. *Science* **324**, 1670–1673.

[5] Visvader JE (2011). Cells of origin in cancer. *Nature* **469**, 314–322.

[6] Singh SK, Clarke ID, Terasaki M, Bonn VE, Hawkins C, Squire J, and Dirks PB (2003). Identification of a cancer stem cell in human brain tumors. *Cancer Res* **63**, 5821–5828.

[7] Singh SK, Hawkins C, Clarke ID, Squire JA, Bayani J, Hide T, Henkelman RM, Cusimano MD, and Dirks PB (2004). Identification of human brain tumour initiating cells. *Nature* **432**, 396–401.

[8] Wang J, Sakariassen PO, Tsinkalovsky O, Immervoll H, Boe SO, Svendsen A, Prestegarden L, Rosland G, Thorsen F, Stuhr L, et al. (2008). CD133 negative glioma cells form tumors in nude rats and give rise to CD133 positive cells. *Int J Cancer* **122**, 761–768.

[9] Joo KM, Kim SY, Jin X, Song SY, Kong DS, Lee JI, Jeon JW, Kim MH, Kang BG, Jung Y, et al. (2008). Clinical and biological implications of CD133-positive and CD133-negative cells in glioblastomas. *Lab Invest* **88**, 808–815.

[10] Shmelkov SV, Butler JM, Hooper AT, Hormigo A, Kushner J, Milde T, St Clair R, Baljevic M, White I, Jin DK, et al. (2008). CD133 expression is not restricted to stem cells, and both CD133+ and CD133− metastatic colon cancer cells initiate tumors. *J Clin Invest* **118**, 2111–2120.

[11] Ogden AT, Waziri AE, Lochhead RA, Fusco D, Lopez K, Ellis JA, Kang J, Assanah M, McKhann GM, Sisti MB, et al. (2008). Identification of A2B5+ CD133− tumor-initiating cells in adult human gliomas. *Neurosurgery* **62**, 505–514; discussion 514-505.

[12] Chen R, Nishimura MC, Bumbaca SM, Kharbanda S, Forrest WF, Kasman IM, Greve JM, Soriano RH, Gilmour LL, Rivers CS, et al. (2010). A hierarchy of self-renewing tumor-initiating cell types in glioblastoma. *Cancer Cell* **17**, 362–375.

[13] Read TA, Fogarty MP, Markant SL, McLendon RE, Wei Z, Ellison DW, Febbo PG, and Wechsler-Reya RJ (2009). Identification of CD15 as a marker for tumor-propagating cells in a mouse model of medulloblastoma. *Cancer Cell* **15**, 135–147.

[14] Ward RJ, Lee L, Graham K, Satkunendran T, Yoshikawa K, Ling E, Harper L, Austin R, Nieuwenhuis E, Clarke ID, et al. (2009). Multipotent CD15+ cancer stem cells in *patched-1*–deficient mouse medulloblastoma. *Cancer Res* **69**, 4682–4690.

[15] Gupta PB, Fillmore CM, Jiang G, Shapira SD, Tao K, Kuperwasser C, and Lander ES (2011). Stochastic state transitions give rise to phenotypic equilibrium in populations of cancer cells. *Cell* **146**, 633–644.

[16] Giese A, Bjerkvig R, Berens ME, and Westphal M (2003). Cost of migration: invasion of malignant gliomas and implications for treatment. *J Clin Oncol* **21**, 1624–1636.

[17] Greig NH (1987). Optimizing drug delivery to brain tumors. *Cancer Treat Rev* **14**, 1–28.

[18] Bao S, Wu Q, McLendon RE, Hao Y, Shi Q, Hjelmeland AB, Dewhirst MW, Bigner DD, and Rich JN (2006). Glioma stem cells promote radioresistance by preferential activation of the DNA damage response. *Nature* **444**, 756–760.

[19] Blazek ER, Foutch JL, and Maki G (2007). Daoy medulloblastoma cells that express CD133 are radioresistant relative to CD133– cells, and the CD133+ sector is enlarged by hypoxia. *Int J Radiat Oncol Biol Phys* **67**, 1–5.

[20] Eyler CE and Rich JN (2008). Survival of the fittest: cancer stem cells in therapeutic resistance and angiogenesis. *J Clin Oncol* **26**, 2839–2845.

[21] Liu G, Yuan X, Zeng Z, Tunici P, Ng H, Abdulkadir IR, Lu L, Irvin D, Black KL, and Yu JS (2006). Analysis of gene expression and chemoresistance of CD133+ cancer stem cells in glioblastoma. *Mol Cancer* **5**, 67.

[22] Singh A and Settleman J (2010). EMT, cancer stem cells and drug resistance: an emerging axis of evil in the war on cancer. *Oncogene* **29**, 4741–4751.

[23] Mani SA, Guo W, Liao MJ, Eaton EN, Ayyanan A, Zhou AY, Brooks M, Reinhard F, Zhang CC, Shipitsin M, et al. (2008). The epithelial-mesenchymal transition generates cells with properties of stem cells. *Cell* **133**, 704–715.

[24] Pang R, Law WL, Chu AC, Poon JT, Lam CS, Chow AK, Ng L, Cheung LW, Lan XR, Lan HY, et al. (2010). A subpopulation of CD26+ cancer stem cells with metastatic capacity in human colorectal cancer. *Cell Stem Cell* **6**, 603–615.

[25] Weber K, Paulus W, and Senner V (2010). The side population of gliomas exhibits decreased cell migration. *J Neuropathol Exp Neurol* **69**, 623–631.

[26] Molina JR, Hayashi Y, Stephens C, and Georgescu MM (2010). Invasive glioblastoma cells acquire stemness and increased Akt activation. *Neoplasia* **12**, 453–463.

[27] Werbowetski-Ogilvie TE, Morrison LC, Fiebig-Comyn A, and Bhatia M (2012). *In vivo* generation of neural tumors from neoplastic pluripotent stem cells models early human pediatric brain tumor formation. *Stem Cells* **30**, 392–404.

[28] Del Duca D, Werbowetski T, and Del Maestro RF (2004). Spheroid preparation from hanging drops: characterization of a model of brain tumor invasion. *J Neurooncol* **67**, 295–303.

[29] Werbowetski-Ogilvie TE, Seyed Sadr M, Jabado N, Angers-Loustau A, Agar NY, Wu J, Bjerkvig R, Antel JP, Faury D, Rao Y, et al. (2006). Inhibition of medulloblastoma cell invasion by Slit. *Oncogene* **25**, 5103–5112.

[30] Northcott PA, Korshunov A, Witt H, Hielscher T, Eberhart CG, Mack S, Bouffet E, Clifford SC, Hawkins CE, French P, et al. (2011). Medulloblastoma comprises four distinct molecular variants. *J Clin Oncol* **29**, 1408–1414.

[31] Taylor MD, Northcott PA, Korshunov A, Remke M, Cho YJ, Clifford SC, Eberhart CG, Parsons DW, Rutkowski S, Gajjar A, et al. (2012). Molecular subgroups of medulloblastoma: the current consensus. *Acta Neuropathol* **123**, 465–472.

[32] Doetsch F, Petreanu L, Caille I, Garcia-Verdugo JM, and Alvarez-Buylla A (2002). EGF converts transit-amplifying neurogenic precursors in the adult brain into multipotent stem cells. *Neuron* **36**, 1021–1034.

[33] Calaora V, Chazal G, Nielsen PJ, Rougon G, and Moreau H (1996). mCD24 expression in the developing mouse brain and in zones of secondary neurogenesis in the adult. *Neuroscience* **73**, 581–594.

[34] Uchida N, Buck DW, He D, Reitsma MJ, Masek M, Phan TV, Tsukamoto AS, Gage FH, and Weissman IL (2000). Direct isolation of human central nervous system stem cells. *Proc Natl Acad Sci USA* **97**, 14720–14725.

[35] Pruszak J, Ludwig W, Blak A, Alavian K, and Isacson O (2009). CD15, CD24, and CD29 define a surface biomarker code for neural lineage differentiation of stem cells. *Stem Cells* **27**, 2928–2940.

[36] Chen Y, Zeng J, Cen L, Wang X, Yao G, Wang W, Qi W, and Kong K (2009). Multiple roles of the p75 neurotrophin receptor in the nervous system. *J Int Med Res* **37**, 281–288.

[37] Johnston AL, Lun X, Rahn JJ, Liacini A, Wang L, Hamilton MG, Parney IF, Hempstead BL, Robbins SM, Forsyth PA, et al. (2007). The p75 neurotrophin receptor is a central regulator of glioma invasion. *PLoS Biol* **5**, e212.

[38] Wang L, Rahn JJ, Lun X, Sun B, Kelly JJ, Weiss S, Robbins SM, Forsyth PA, and Senger DL (2008). Gamma-secretase represents a therapeutic target for the treatment of invasive glioma mediated by the p75 neurotrophin receptor. *PLoS Biol* **6**, e289.

[39] Barnes M, Eberhart CG, Collins R, and Tihan T (2009). Expression of p75NTR in fetal brain and medulloblastomas: evidence of a precursor cell marker and its persistence in neoplasia. *J Neurooncol* **92**, 193–201.

[40] Yang ZJ, Ellis T, Markant SL, Read TA, Kessler JD, Bourboulas M, Schuller U, Machold R, Fishell G, Rowitch DH, et al. (2008). Medulloblastoma can be initiated by deletion of Patched in lineage-restricted progenitors or stem cells. *Cancer Cell* **14**, 135–145.

[41] Schuller U, Heine VM, Mao J, Kho AT, Dillon AK, Han YG, Huillard E, Sun T, Ligon AH, Qian Y, et al. (2008). Acquisition of granule neuron precursor identity is a critical determinant of progenitor cell competence to form Shh-induced medulloblastoma. *Cancer Cell* **14**, 123–134.

[42] Wang X, Cui M, Wang L, Chen X, and Xin P (2010). Inhibition of neurotrophin receptor p75 intramembran proteolysis by gamma-secretase inhibitor reduces medulloblastoma spinal metastasis. *Biochem Biophys Res Commun* **403**, 264–269.

[43] Meletis K, Wirta V, Hede SM, Nister M, Lundeberg J, and Frisen J (2006). p53 suppresses the self-renewal of adult neural stem cells. *Development* **133**, 363–369.

[44] Pasquale EB (2008). Eph-ephrin bidirectional signaling in physiology and disease. *Cell* **133**, 38–52.

[45] Lim YS, McLaughlin T, Sung TC, Santiago A, Lee KF, and O'Leary DD (2008). p75(NTR) mediates ephrin-A reverse signaling required for axon repulsion and mapping. *Neuron* **59**, 746–758.

[46] Naska S, Lin DC, Miller FD, and Kaplan DR (2010). p75NTR is an obligate signaling receptor required for cues that cause sympathetic neuron growth cone collapse. *Mol Cell Neurosci* **45**, 108–120.

[47] Nakada M, Niska JA, Miyamori H, McDonough WS, Wu J, Sato H, and Berens ME (2004). The phosphorylation of EphB2 receptor regulates migration and invasion of human glioma cells. *Cancer Res* **64**, 3179–3185.

[48] Hoelzinger DB, Mariani L, Weis J, Woyke T, Berens TJ, McDonough WS, Sloan A, Coons SW, and Berens ME (2005). Gene expression profile of glioblastoma multiforme invasive phenotype points to new therapeutic targets. *Neoplasia* **7**, 7–16.

[49] Miao H, Li DQ, Mukherjee A, Guo H, Petty A, Cutter J, Basilion JP, Sedor J, Wu J, Danielpour D, et al. (2009). EphA2 mediates ligand-dependent inhibition and ligand-independent promotion of cell migration and invasion via a reciprocal regulatory loop with Akt. *Cancer Cell* **16**, 9–20.

[50] Sikkema AH, den Dunnen WF, Hulleman E, van Vuurden DG, Garcia-Manero G, Yang H, Scherpen FJ, Kampen KR, Hoving EW, Kamps WA, et al. (2012). EphB2 activity plays a pivotal role in pediatric medulloblastoma cell adhesion and invasion. *Neuro Oncol* **14**, 1125–1135.

[51] Wang SD, Rath P, Lal B, Richard JP, Li Y, Goodwin CR, Laterra J, and Xia S (2012). EphB2 receptor controls proliferation/migration dichotomy of glioblastoma by interacting with focal adhesion kinase. *Oncogene* **31**, 5132–5143.

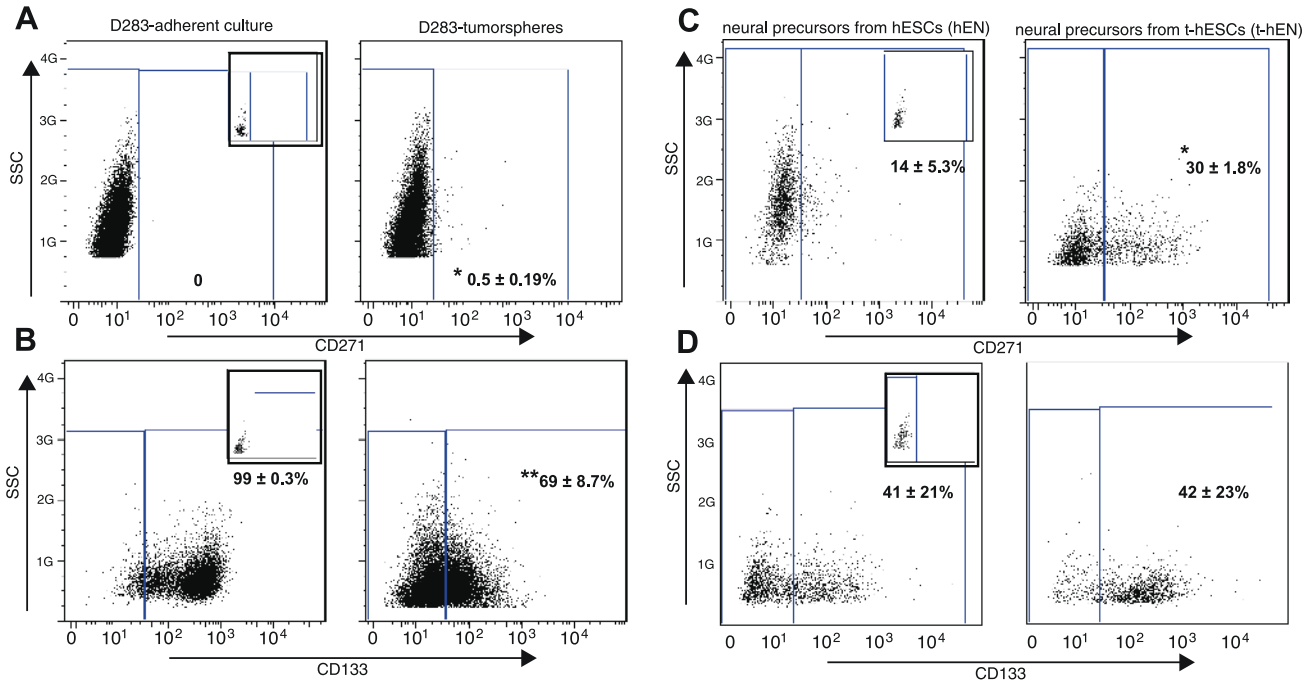

Figure W1. CD271 is enriched in tumor sphere culture and highly self-renewing MB subpopulations from multiple cell lines. (A, B) D283 parental adherent cultures grown in 10% FBS (left panels) do not express CD271 but exhibit high levels of CD133 expression by flow cytometry. Following culture as tumor spheres in BTPC conditions, D283 begin to exhibit a small but consistent significant subpopulation of CD271+ cells. CD133 expression is significantly decreased. Insets: live cell–only controls; $N = 5$ independent experiments. (C, D) CD271 levels (C) are significantly higher in t-hENs relative to normal hENs. CD133 is unchanged t-hENs *versus* hENs (D); $N = 3$ independent experiments.

A

Diseases and Disorders

Name	p-value	# Molecules
Cancer	6.24E-18 - 1.28E-04	114
Neurological Disease	3.71E-15 - 1.12E-04	82
Psychological Disorders	3.71E-15 - 2.15E-05	50
Connective Tissue Disorders	6.07E-15 - 9.81E-06	51
Inflammatory Disease	6.07E-15 - 4.41E-05	62

Molecular and Cellular Functions

Name	p-value	# Molecules
Cellular Movement	1.17E-22 - 1.15E-04	84
Cell-To-Cell Signaling and Interaction	3.95E-15 - 1.20E-04	72
Cellular Growth and Proliferation	1.95E-13 - 8.68E-05	97
Cell Death and Survival	1.95E-10 - 1.28E-04	81
Cellular Development	2.39E-10 - 1.28E-04	97

B

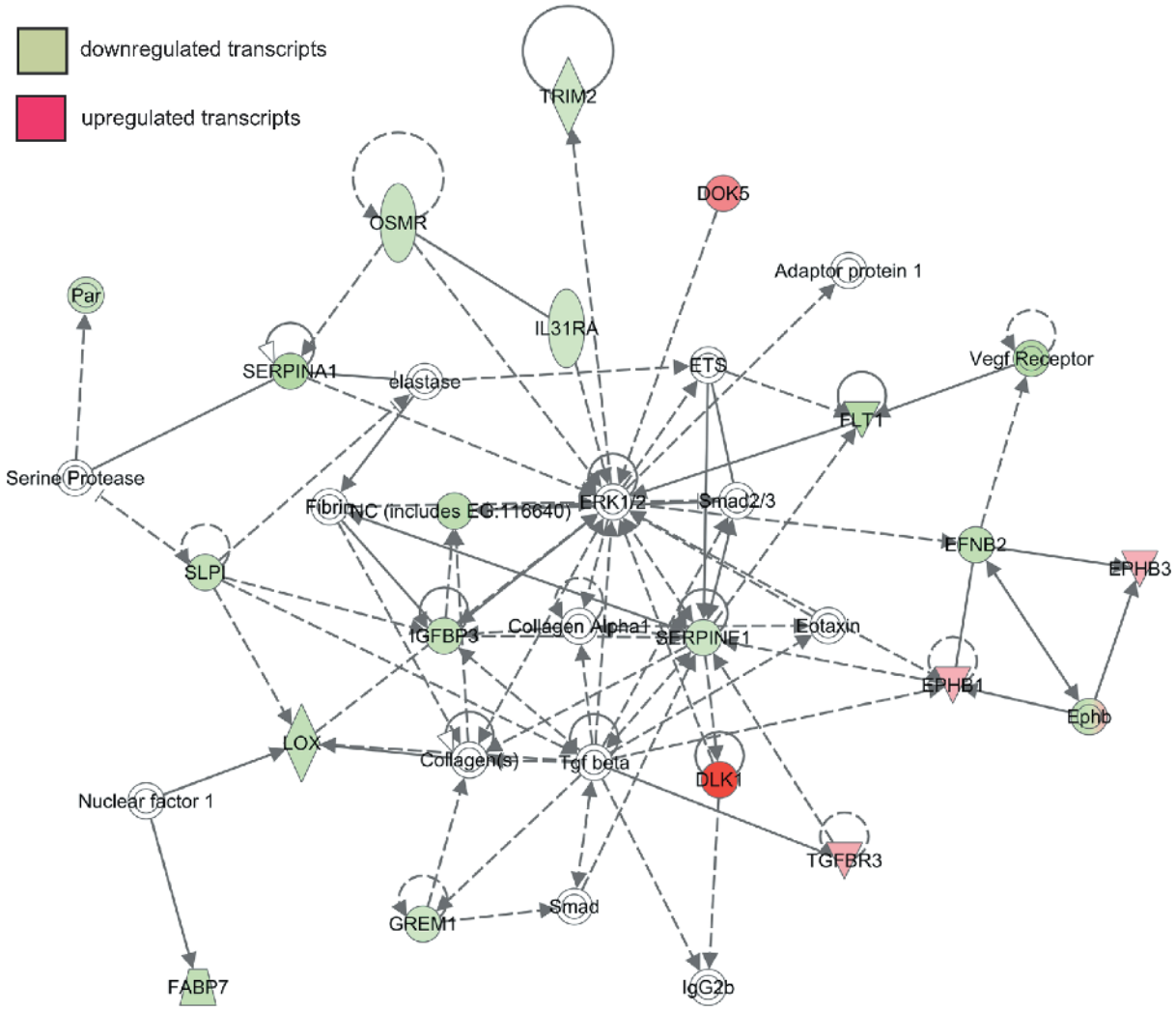

Figure W2. Top diseases, molecular/cellular functions, and networks dysregulated in higher *versus* lower self-renewing MB tumor spheres. (A) Top diseases (upper panel) and molecular and cellular functions (lower panel) dysregulated in higher self-renewing *versus* lower self-renewing tumor spheres. (B) Top dysregulated cellular network consisting of molecules associated with cellular movement. Note the presence of EPHB receptors and ephrin B2 ligand. Shaded green areas denote transcripts that are significantly downregulated and red areas denote significantly upregulated transcripts in higher self-renewing *versus* lower self-renewing tumor spheres.

Table W4. Primer Sequences Used for qPCR Reactions.

Gene	Forward Sequence	Reverse Sequence	Product (bp)
Ephrin B2	5′-GTT CGA CAA CAA GTC CCT TTG-3′	5′-CTG AAG CAA TCC CTG CAA ATA-3′	123
EPHB1	5′-GGA AAC GGG CTT ATA GCA AAG-3′	5′-TCG TAA GTG AAG GGG TCA ATG-3′	110
EPHB2	5′-GAC TCC ACT ACA GCG ACT GCT-3′	5′-TCT CAT CGT AGC CAC TCA CCT-3′	82
EPHB3	5′-TTG TCA ATA CCC TGG ACA AGC-3′	5′-AAT CAC CAA CTG TCG TGA AGG-3′	135
EPHB4	5′-AAT GTC ACC ACT GAC CGA GAG-3′	5′-ATT TGA CCT CGT AGT CCA GCA-3′	136
EPHB6	5′-AAT AGC CAC TTG GTG TGC AAG-3′	5′-CAT GAG TAT CCC AAA GCT CCA-3′	144
Otx2	5′-GAG GTG GCA CTG AAA ATC AAC-3′	5′-TCT TCT TTT TGG CAG GTC TCA-3′	136
Sox1	5′-TGG ATG AAG GAC AAA GAC CAG-3′	5′-GTT TTG GTT CAG CGA TTG TGT-3′	116
βIII tubulin	5′-GGC CTT TGG ACA TCT CTT CA-3′	5′-TCG CAG TTT TCA CAC TCC TTC-3′	147

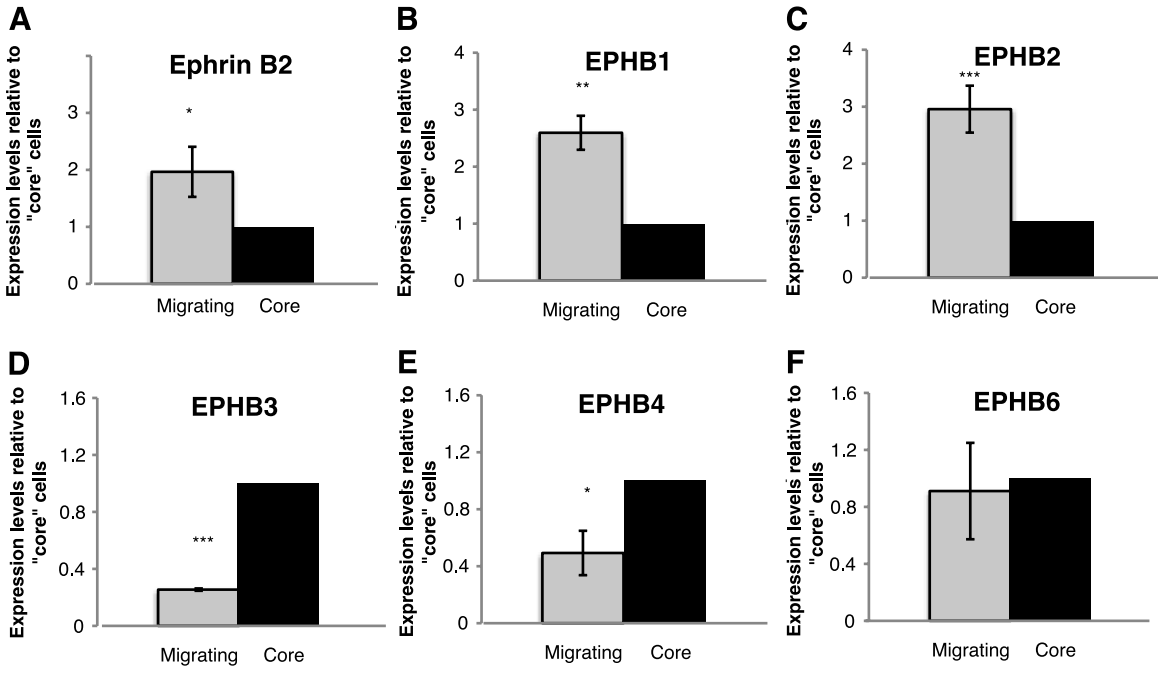

Figure W3. The Eph-ephrin signaling pathway is dysregulated in migrating *versus* core MB cells. (A–F) qPCR analysis of the ephrin B2 ligand and EPHB1, B2, B3, B4, and B6 receptors in "core" *versus* "migrating" Daoy MB cells. Note the up-regulation of ephrin B2, EPHB1, and EPHB2 and significant down-regulation of EPHB3 and EPHB4 in "migrating" *versus* "core" cells. Error bars, SEM; *$P <$ .05, **$P <$ .01, ***$P <$ .001.